Spin-selective scattering modes in a disordered anisotropic optical medium

Ankit Kumar Singh [1,*] Antariksha Das [1,2] Sourin Das,[1] and Nirmalya Ghosh[1]
[1]*Indian Institute of Science Education and Research Kolkata, Mohanpur 741246, India*
[2]*QuTech, Delft University of Technology, 2628 CJ Delft, The Netherlands*

(Received 24 February 2020; accepted 27 August 2020; published 21 September 2020)

The geometric and dynamic phases have competing effects as far as the scattering of light from an inhomogeneous anisotropic optical medium is concerned. If fine-tuned appropriately, these effects can completely cancel each other for a chosen spin component while having an additive effect on the orthogonal component. Here, we show a manifestation of extraordinary spin-selective modes in the Fourier spectrum of a Gaussian beam transmitted through an anisotropic disordered medium. We realize the concept by using a twisted nematic liquid-crystal-based spatial light modulator with random gray-level distributions for an incident Gaussian beam.

DOI: 10.1103/PhysRevA.102.033518

I. INTRODUCTION

Spin-orbit coupling refers to the relativistic interaction of a particle's spin degree of freedom with its orbital degree of freedom. The coupling is associated with the breaking of the spatial inversion symmetry of the system. Spin-orbit-coupled systems have been observed in diverse fields of physics, and at different scales, spanning from atomic, condensed-matter systems to optical systems. In optics, coupling or interconversion of the spin angular momentum of a light beam (related to the polarization of light) with its orbital angular momentum (related to a helical or twisted wavefront) goes by the name of spin-orbit interaction (SOI) of light and is a topic of recent interest [1–13]. The conservation of the total angular momentum of a light beam leads to the generation of geometric phase and its spatial gradient, which is related to all the optical SOI phenomena in cyclic as well as noncyclic processes [1,1–16]. Some of the very interesting effects arising from such ubiquitous interactions are the spin Hall effect (SHE) of light from a spatially tailored anisotropic medium, the optical Rashba effect, the spin-dependent scattering of light, etc. [1–8,10,11]. Moreover, the intriguing phenomenon has a wide range applications as it can offer a new direction towards the development of spin-controlled photonic devices ranging from the spin-controlled directionality to the spin-controlled orbital-angular-momentum generation [1–3,17–19].

Most of the cases discussed above are of ordered systems. In this regard, it was recently shown that, for a completely disordered inhomogeneous anisotropic optical system, one could get spin-orbit-coupled random scattering modes over the entire momentum domain, which can be characterized as the random optical Rashba effect [13]. The origin of such an effect can be interpreted as the disorder in the spatial distribution of geometric phase (and hence geometric phase gradient) or the disordered strength of spin-orbit coupling across the beam profile. The interplay of disorder and SOI in a medium aspires to build synthetic electromagnetic materials that are capable of hosting the topological states required for topological photonics.

Here, we report a remarkable effect that can originate from a perfect synchrony associated with the spatial distribution of anisotropy of a medium and SOI of light. The disordered anisotropic systems can demonstrate an input-spin-selective or spin asymmetric random scattering modes, i.e., the randomly scattered modes are observed for one spin state only. In contrast, the other spin state follows an entirely different trajectory with almost no effect of the system's disorder. This unprecedented control of the spin-orbit coupling of light in the disordered medium can significantly impact the exploration of optical mediums for "topological photonics." The findings can also be implicated in various other domains such as optical, quantum, and condensed-matter systems to have vivid applications.

This paper is organized in the following way: in Sec. II, the theory behind the spin-orbit interaction of light in a spatially disordered inhomogeneous anisotropic medium is discussed. The effect of randomness strength in spatial phase distribution and incident Gaussian beam width on the transition of the spin-orbit effect from optical spin Hall to random optical Rashba effect is studied. Subsequently, we propose a system that can be used to obtain the spin-dependent random scattering modes over the entire momentum domain in a spatially disordered inhomogeneous anisotropic medium with a uniformly randomized spatial phase gradient. In Sec. III, we experimentally show the spin-dependent random scattering modes by using a spatial light modulator that can simultaneously tune the dynamical and geometrical phase distribution. In Sec. IV, we summarize our results with their possible future implications.

II. THEORY

When a circularly polarized Gaussian beam [$G(x, y) = e^{-(x^2+y^2)/w_o^2}$, w_o is the beam width] propagates through a spatially inhomogeneous anisotropic medium, it acquires a phase distribution $\phi(x, y)$ that creates a spatial phase gradient transverse to the beam propagation direction [1–7,13,17].

*aks13ip027@iiserkol.ac.in

The anisotropic medium also introduces changes in the polarization state of the incident light depending on the spatial distribution of anisotropy elements. Here, we only consider the anisotropic elements to be a phase anisotropic half-wave plate (for simplicity) oriented at random angles throughout the space. The anisotropic medium composed of half-wave plates projects the incident circularly polarized state to the orthogonal circularly polarized state. It also imparts a spatially varying geometric phase distribution dependent on the distribution of orientation angles of the anisotropy axis of the half-wave plate. Assuming no depolarization and no change in the electric-field amplitude in the interaction, the electric field ($\mathbf{E_t}$) transmitted from the inhomogeneous medium can be written as

$$\mathbf{E_t} = e^{i\phi(x,y)} G(x,y)|+/-\rangle. \tag{1}$$

Here, $|+/-\rangle$ indicates the transmitted right/left circular polarized (RCP/LCP) state of light that is orthogonal to the incident circularly polarized state. The phase ϕ [$= \pm\phi_g(x,y) + \phi_d(x,y)$] is the spatially varying total phase [sum of the dynamical (ϕ_d) and the geometrical phases $\pm\phi_g$, $+(-)$ for RCP (LCP) state of light)] acquired by the light beam. The breaking of spatial inversion symmetry of the system by the inhomogeneous distribution of the total phase leads to the SOI of light [1–7,13,17]. The strength of such an effect depends on the phase inhomogeneity acquired by the light beam.

In case the total phase is entirely geometrical ($\phi = \pm\phi_g$) and varies randomly in space [13], a complex transverse momentum ($\mathbf{k}_\perp$, k_x, and k_y) distribution of the field can be observed with the $\mathbf{k}_\perp$ values distributed throughout the momentum space as

$$I_t(k_x, k_y) = \left| \iint_{-\infty}^{+\infty} e^{-i(k_x x + k_y y)} \mathbf{E_t}(x,y)\, dx\, dy \right|^2. \tag{2}$$

The above equation corresponds to the intensity of the spin *symmetric* random scattering modes [i.e., $I_t^{\mathrm{LCP}}(k) = I_t^{\mathrm{RCP}}(-k)$] in the momentum space due to the opposite sign of the geometrical phase $\phi_g(x,y)$ acquired by the LCP and RCP polarizations [1,2,4–7,13]. However, the dynamical phase does not follow such symmetries for the circular polarization states transmitted through linear retarders [19]. Thus, a spatially varying geometrical and dynamical phase would give rise to spin *asymmetric* random scattering modes [i.e., $I_t^{\mathrm{LCP}}(k) \neq I_t^{\mathrm{RCP}}(-k)$] in the momentum space. The spin asymmetricity I_{sa} of the random scattering modes in such system can be quantified as

$$I_{sa} = \left\langle \frac{\left| I_t^{\mathrm{LCP}}(k_x,k_y) - I_t^{\mathrm{RCP}}(-k_x,-k_y) \right|}{I_t^{\mathrm{LCP}}(k_x,k_y) + I_t^{\mathrm{RCP}}(-k_x,-k_y)} \right\rangle, \tag{3}$$

where $\langle \ldots \rangle$ denotes a sum over all the $k_\perp$ values.

The SOIs from such disordered inhomogeneous anisotropic medium can also be understood in terms of the spatial autocorrelation function $A(x,y)$ of the electric field transmitted from the disordered medium. The autocorrelation $A(x,y)$ of the transmitted field can be related to the momentum distribution of the field intensity (power spectrum) through the *Wiener-Khinchin Theorem* as

$$I_t(k_x, k_y) = \iint_{-\infty}^{+\infty} e^{-i(k_x x + k_y y)} A(x,y)\, dx\, dy. \tag{4}$$

It implies that a complex-valued autocorrelation function that changes randomly in space has all the spatial frequency components with varying amplitude, leading to the generation of random scattering modes in the Fourier plane.

A RCP Gaussian beam of beam width $w_o = 80d$ (d is the size of the individual anisotropic element or the minimum length having a constant phase) is passed through the spatially disordered anisotropic medium. It is worth mentioning that the findings are independent of the exact value of d as long as the transmitted field can be described by Eq. (1). The value of w_o/d gives a measure of the effective number of random elements encountered by the beam while propagation through the anisotropic medium, which determines the momentum space intensity distribution. In Fig. 1(a), we have shown a one-dimensional spatial distribution of geometric phase ϕ_g with randomized phase gradients, which is obtained by the RCP Gaussian beam ($w_o = 80d$) when it is passed through the anisotropic medium. The geometric phase $\phi_g(x)$ is chosen to be a delta correlated uniformly distributed random function [$f^\epsilon(\phi_g) = 1/2\pi\epsilon$ for $-\epsilon\pi \leqslant \phi_g(x) < \epsilon\pi$ otherwise $f^\epsilon(\phi_g) = 0$, $0 \leqslant \epsilon \leqslant 1$ is the amplitude of randomness] of x coordinate with $\epsilon = 1$, see Figs. 1(a) and 1(b). Hence, the spin-orbit-coupled modes are seen along the k_x axis in the momentum space. Completely spin symmetric [$I_t^{\mathrm{LCP}}(k_x) = I_t^{\mathrm{RCP}}(-k_x)$), $I_{sa} = 0$] random scattering modes in the momentum space are obtained for the LCP and RCP polarization state, as shown in Fig. 1(c). The momentum scale in the figure and for all further discussions are normalized with the wave number of the incident Gaussian beam. It is to be noted that even an optimally spaced binary distribution is enough to observe the phenomenon, as shown in Appendix B.

The scattering field profile from the random anisotropic system was studied with a varying width (w_o) of the input beam and the amplitude of randomness (ϵ). The response was studied for over 100 samples. The cyan-colored region in Fig. 2 shows the parameters of the system for which the random modes of sufficiently large amplitude (0.15 times the maximum intensity or more) are observed in momentum-space intensity distribution for more than half of the samples. The curve marks the limits of beam width (w_o) and amplitude of randomness (ϵ) parameters that lead to a transition from the usual momentum domain spin Hall effect (green) to spin-orbit-coupled random modes (cyan) for more than half of the cases. It is to be noted that the nature of the curve remains the same for the criterion set to even larger amplitude of the random modes than the chosen amplitude ($\geqslant$0.15). However, it shifts towards more randomness in the phase distribution (larger ϵ) for the larger chosen amplitude. Nevertheless, it is clear from the figure that the reduced beam width can be used to obtain the random modes even for the smaller amplitude of randomness.

The symmetric nature of spin-orbit-coupled random modes in the Fourier space is guaranteed if the total phase distribution has only the geometrical phase contribution. An additional spatially disordered dynamical phase distribution

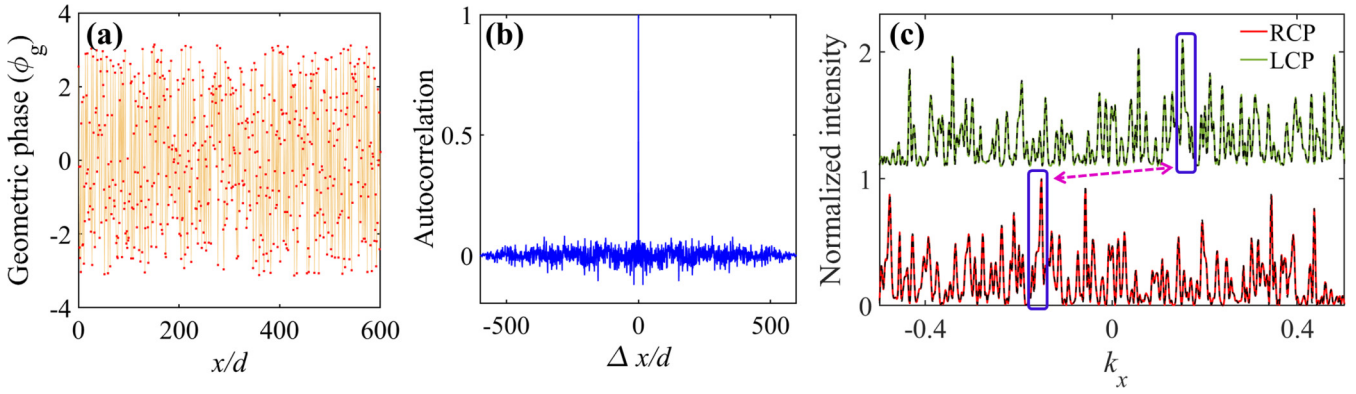

FIG. 1. The spin-symmetric random scattering modes from a uniformly randomized geometric phase distribution. (a) The geometric phase distribution for RCP polarization state obtained from the anisotropic medium (amplitude of randomness $\epsilon = 1$) disordered along the x direction. (b) The two-point autocorrelation of the geometric phase distribution as a of function of the distance between the points $\Delta x/d$. (c) The momentum space intensity distribution for LCP and RCP polarization states along k_x, showing the spin-symmetric random scattering modes $[I_t^{\mathrm{LCP}}(k) = I_t^{\mathrm{RCP}}(-k)]$ for a Gaussian beam of width $w_o = 80d$ [calculated by using Eq. (2) (solid line) and Eq. (4) (dashed line)]. The intensity of the LCP state is shifted for better visualization.

breaks the spin symmetry of the random scattering modes and an *asymmetric* scattering mode ($I_{sa} > 0$) is observed from the disordered anisotropic medium. The *asymmetric* scattering from the disordered medium can be used to actively tune the random scattering modes by using an elliptical polarization state of light to deferentially excite the LCP and RCP scattering modes, as shown in Figs. 3(a)–3(d). However, when the geometrical and dynamical phase acquired from the disordered system is synchronous (i.e., a perfect zero-order correlation between the two-phase distribution) and of similar magnitude [e.g., $\phi_d(x) \approx \phi_g(x) + \text{const.}$], then the randomly scattered modes are observed for RCP, while the LCP shows no effect of the disordered medium, as shown in Fig. 3(a). This *extraordinary spin asymmetric* random scattering mode

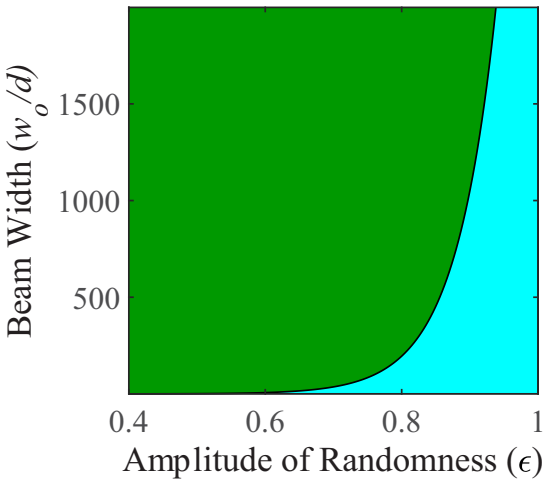

FIG. 2. The effect of the beam width of the input Gaussian beam (w_o) and the amplitude of randomness (ϵ) of the disordered anisotropic system on the Fourier space intensity distribution is shown. The curve marks the boundary of the transition from the usual momentum domain spin Hall effect (green) to spin-orbit-coupled random scattering modes (cyan) with varying beam width and amplitude of randomness.

[Figs. 3(a)–3(c)] arise due to a zero total phase $[\pm\phi_g(x) + \phi_d]$ gradient for LCP polarization state. At the same time, the RCP gets a phase gradient twice the acquired geometric phase gradient, as can be noted from the frequency distribution of the total phase value for RCP and LCP polarization states [Figs. 3(e), 3(g), 3(i), and 3(k)]. An asynchronous dynamical and geometrical phase distribution gives rise to the *asymmetric* random scattered momentum modes for all the elliptical polarization states of light, as shown in Figs. 3(b) and 3(d). However, the strength of random modes observed for asynchronous systems depends on the amplitude of randomness of the phase distribution and the input beam width.

III. EXPERIMENT AND RESULTS

In this section, we experimentally demonstrate the spin-selective or spin asymmetric random scattering modes in an optical system. It can be done in a twisted nematic-liquid-crystal-based transmissive spatial light modulator (SLM, Holoeye LC 2002). In this particular type of SLM, the effective retardance value (the dynamical phase) and the orientation angle (i.e., the Panchratanam-Berry geometric phase) of each equivalent retarder can be simultaneously tuned in a synchronous manner by varying the voltage applied (projected gray-level value n on the SLM) across the pixels of the SLM. The maximum amplitude of randomness that can be reached in such a system is significantly less, as the phase retardance of SLM can be varied from $\pi/7$ to $\approx 3\pi/4$ rad and the effective orientation can be simultaneously tuned from 0 to $2\pi/5$ rad (see Appendix C) [6]. It is worth mentioning that the SLM also introduces a small depolarization effect ($\approx$0.1) on the light transmitted from the system that leads to a small amount of unpolarized light transmitted from the SLM [20]. Despite this, the randomly scattered modes from the SLM can be observed with a beam of sufficiently small effective beam width and the remaining ($\approx$90%) of transmitted light carries the signature of the polarized interaction from the SLM. The 8×8 pixel bins (pixel pitch ≈ 32 μm) were assigned a single value of the gray level to reduce the effective beam width [w_o/(size of the bin)]. The gray-level values $[n = 60 f(\epsilon_{\mathrm{slm}}) +$

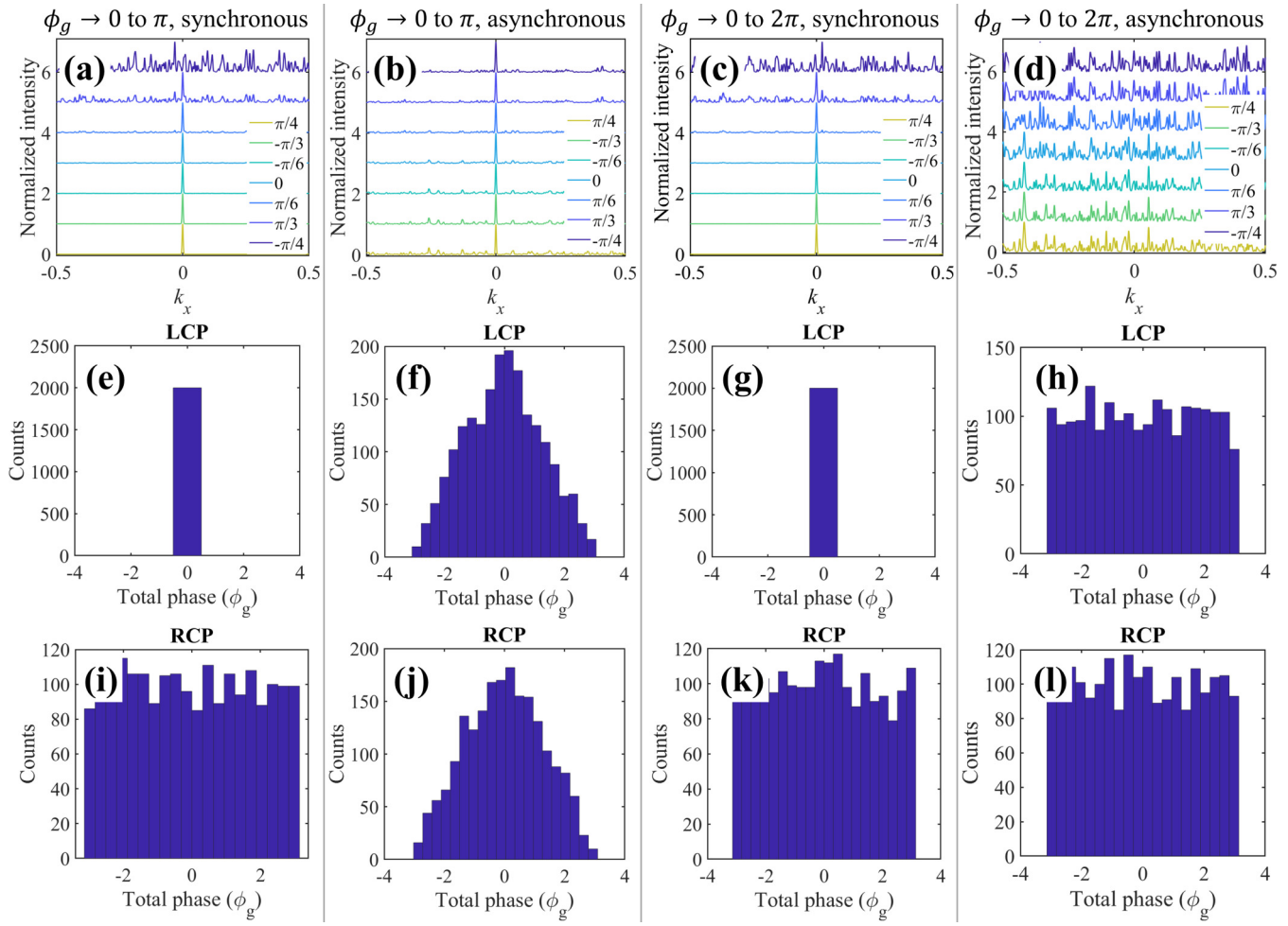

FIG. 3. The polarization-controlled tuning of momentum-space intensity distribution in synchronous and asynchronous systems. (a)–(d) The elliptical polarization states ($[1, e^{i\delta}]^T$, ellipticity $\delta/2$ is mentioned in legends] were used to actively tune the momentum-space intensity distribution from the asymmetric random scattering system for an input Gaussian beam of width $80d$ (the intensities are shifted for better visualization). The spatially disordered system was taken such that the geometric phase [$\pm\phi_g(x)$, + (−) for RCP (LCP) polarization of light] of the transmitted light is uniformly distributed between (a), (b) $-\pi/2$ to $\pi/2$ and (c), (d) π to π. The momentum-space intensity distribution for (a), (c) synchronous [$\phi_d(x) = \phi_g(x)$], and (b), (d) asynchronous [$\phi_d(x)$ is distributed in same manner as $\phi_g(x)$] systems. The extraordinary spin-selective modes are observed for the synchronous systems. (e)–(l) The total phase-frequency distributions for LCP and RCP states are given below the corresponding normalized intensity distributions of the disordered medium.

80, where $f(\epsilon_{\text{slm}})$ is a uniformly random distribution between $-\epsilon_{\text{slm}}$ and $+\epsilon_{\text{slm}}$, here $0 \leqslant \epsilon_{\text{slm}} \leqslant 1$] were given on the SLM's pixel bins to generate a synchronous disordered anisotropic medium with a random magnitude of the phase retardance and a random orientation angle of the equivalent retarder.

A linearly polarized Gaussian beam [wavelength $\lambda \approx 633$ nm, $w_o = 2.25$ mm or 9 effective units (w_o/d) with respect to the 8×8 bin size] was incident on the SLM with a random phase distribution [random local phase gradient across each bin, a sample image with $\epsilon_{\text{slm}} = 1$ is shown in Fig. 4(b)], and the transmitted light was analyzed by using LCP and RCP polarization projections. The projected beam was focused by using a lens to observe the momentum space distribution at the focal plane. A small disorder was introduced in the gray-level distribution of the SLM to observe the spin Hall effect of light [Fig. 4(c)]. An increase in the amplitude of randomness gives rise to the random scattering modes in the momentum-space distribution for RCP polarization, as shown in Fig. 4(d) for $\epsilon_{\text{slm}} = 1$. The LCP projection gives no such random scattering modes for the same distribution [see inset of Fig. 4(d)]. It shows the extraordinary spin selectivity and asymmetricity of the scattered random modes from the SLM. The spin selectivity is observed due to nearly the same magnitude and synchronous nature of the dynamical and geometrical phases acquired in the SLM. Moreover, as expected, the reduced effective beam width gives rise to more dominant random scattering modes in momentum space [see Fig. 4(e)].

It is important to note that, even for maximum possible spatial randomness in the distribution of the gray level of the SLM, the range of geometric phase distribution is small because of the limited range of the retardance value and the orientation angle of the spatially tunable retarders in the SLM. Hence the need to reduce the effective beam width of the incident beam. The reduced effective beam width of the incident beam leads to a smaller number of random scattering modes observed in momentum space (see Appendix A). However, the range of the retardance value can be enhanced, and

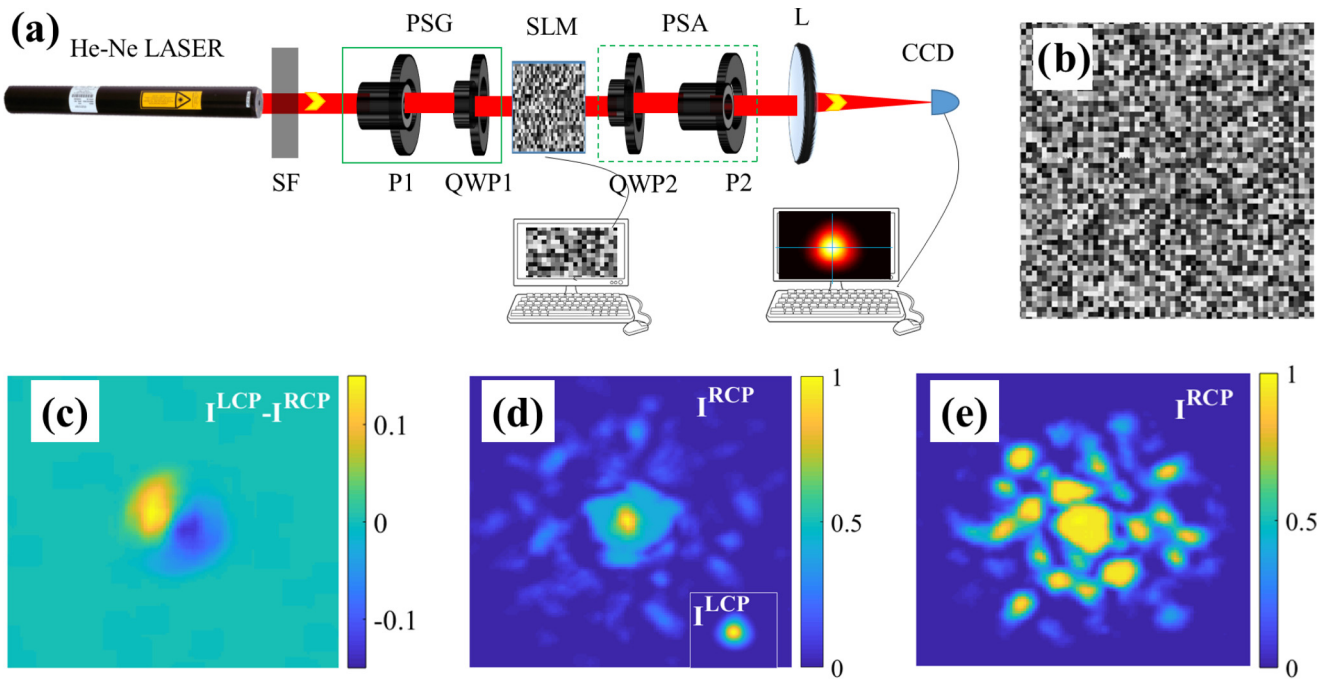

FIG. 4. The experimental demonstration of the spin Hall effect of light and the spin-selective random scattering modes using the spatial light modulator. (a) The experimental setup: a spatially filtered (SF) Gaussian beam (helium-neon) was passed through a polarization-state generator (PSG) consisting of a polarizer (P1) and a quarter-wave plate (QWP1) to generate linearly polarized light. The linearly polarized light was incident on a transmissive SLM whose phase distribution was controlled by using a gray-level image [as shown in panel (b)]. The transmitted light was projected on the LCP and RCP polarization states by using a polarization-state analyzer (PSA). The momentum distribution of LCP and RCP states was measured by using a photodetector (CCD) kept at the focal plane of lens L. (c) The difference between the intensity distribution for LCP and RCP polarization projection for $\epsilon_{slm} = 0.1$ shows the usual momentum-domain spin Hall effect of light, for 8×8 bins. The momentum-space intensity distribution for the RCP polarization projection showing the spin-selective random scattering modes for (d) 8×8 bins (the inset shows no effect of the disorder on the LCP polarization projection) and (e) 15×15 bins, in the SLM.

the depolarizing interactions can be reduced by an appropriately designed liquid-crystal device [21,22]. Additionally, the incident-beam polarization or spatial profile can be tailored to modulate such effects [4,23].

IV. CONCLUSION

It is evident from the above discussion and the experiment that the spin-selective or spin asymmetric random scattering modes can be observed from a disordered anisotropic medium with synchronous dynamical and geometrical phase distributions. The extraordinary spin selectivity of the interplay between the SOI effect and disorder will significantly impact the field of topological photonics. In addition, the controlled active tuning of the randomly scattered modes using the polarization of light may have potential applications in trapping microparticles in a disordered potential [24] and dynamic speckle illumination microscopy [25], with useful implications in the localization of ultracold atoms [26] and super-resolution imaging techniques [27].

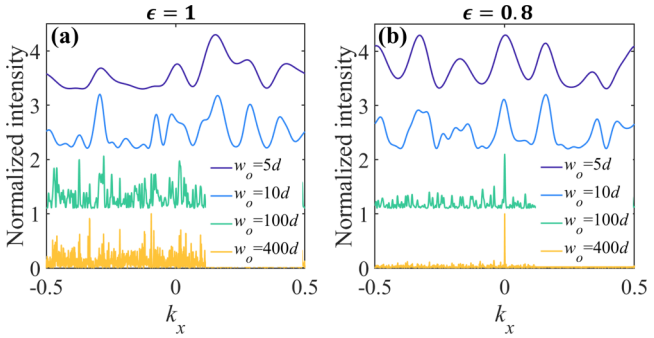

FIG. 5. The momentum-space intensity distribution is shown of the random scattering modes with a varying width of the input Gaussian beam (the momentum scale is normalized by the wave number of the incident beam) for (a) $\epsilon = 1$ and (b) $\epsilon = 0.8$. The intensities are shifted for better visualization.

ACKNOWLEDGMENTS

Authors acknowledge the Indian Institute of Science Education and Research, Kolkata, for the funding and facilities. A.K.S. acknowledges the Council of Scientific and Industrial Research (CSIR), Govt. of India for a research fellowship.

APPENDIX A: THE ROLE OF BEAM WIDTH IN THE AUTOCORRELATION FUNCTION AND MOMENTUM-SPACE INTENSITY DISTRIBUTION

The momentum-space intensity distribution for the RCP input Gaussian beams with various beam width w_o is shown in Fig. 5 for a random geometric phase distribution with $\epsilon = 0.8$ and $\epsilon = 1$. The characteristics of the Fourier space intensity distribution for a system with $\epsilon = 1$ is independent of the

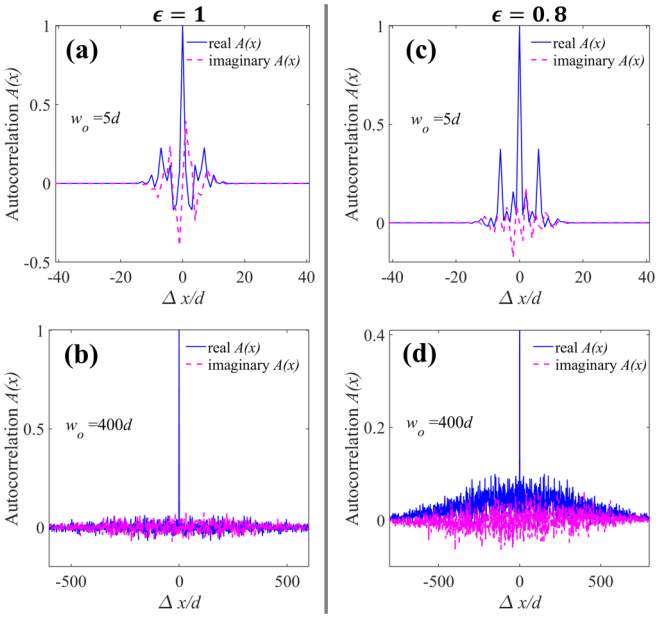

FIG. 6. The autocorrelation of the light transmitted from the inhomogeneous anisotropic medium corresponding to the momentum distribution shown in Fig. 5 for (a), (b) $\epsilon = 1$, and (c), (d) $\epsilon = 0.8$ and input Gaussian beam of width (a), (c) $5d$ and (b), (d) $400d$.

beam width, i.e., the random scattering modes are observed for all values of w_o. However, two different limits of the effect are obtained from the same distribution of geometric phase ($\epsilon = 0.8$) by varying the beam width of the Gaussian input beam, as shown in Fig. 5(b). In the case of $\epsilon = 0.8$, the smaller beam widths show the spin-symmetric random scattering modes (dominated by randomly scattered modes, for $w_o = 5d$ and $10d$). In contrast, the larger beam width shows the usual spin Hall effect of light (dominated by a single Gaussian peak, for $w_o = 400d$) due to the broken inversion symmetry of the inhomogeneous anisotropic structure media from the same system [see Fig. 5(b)]. It gives clear evidence of the role of the beam width of the incident light beam on the effect observed in momentum space for $\epsilon < 1$, i.e., the usual momentum-domain spin Hall effect of light or the spin-symmetric random scattering modes.

It can also be seen from Fig. 5, with the reducing beam width of the Gaussian beam, the density or number of the random scattering modes observed in Fourier space decreases significantly. Such dependence of the number of scattering modes on beam width leads to a small number of the randomly scattered modes observed from the SLM in our experiment, as the effective beam width w_o/d for our system is 9 units.

In Figs. 6(a)–6(d), we have shown the real and imaginary parts of the two-point autocorrelation function (with the distance between the points $\Delta x/d$) of the transmitted beam from the inhomogeneous anisotropic media for various input beam widths. It can be seen that the random medium modifies the spatial autocorrelation function of the input Gaussian beam from a perfect Gaussian function to a random function with various spatial frequency components. The random geometric phase distribution for Figs. 6(a)–6(d) is chosen to be the same as in Fig. 5. Thus, the autocorrelation shown in Fig. 6 is directly related to the momentum space intensity distribution shown in Fig. 5 by a Fourier transform [see Eq. (4)]. The strength of fluctuations in the autocorrelation function dictates the nature of the intensity distribution in Fourier (momentum) space for the random medium. *First*, when the fluctuations in the autocorrelation are large, we observe the "random modes" in the Fourier space intensity distribution due to a large number of frequency components present in the autocorrelation function; see Figs. 6(a)–6(c) and Fig. 5. *Second*, when such fluctuations are small and the Gaussian nature of the autocorrelation function takes over, and we observe a dominantly Gaussian nature of the Fourier space intensity distribution, see Figs. 6(d) and 5(b). However, the intensity distribution is usually not centered at the origin of the transverse momentum space due to the other frequency components present in the autocorrelation function of the transmitted beam leading to the usual spin Hall effect of light (dominated by a single Gaussian peak for a given spin state); see Figs. 6(d) and 5.

Thus, the spatial autocorrelation function is modulated by the beam width of the Gaussian beam incident on the system.

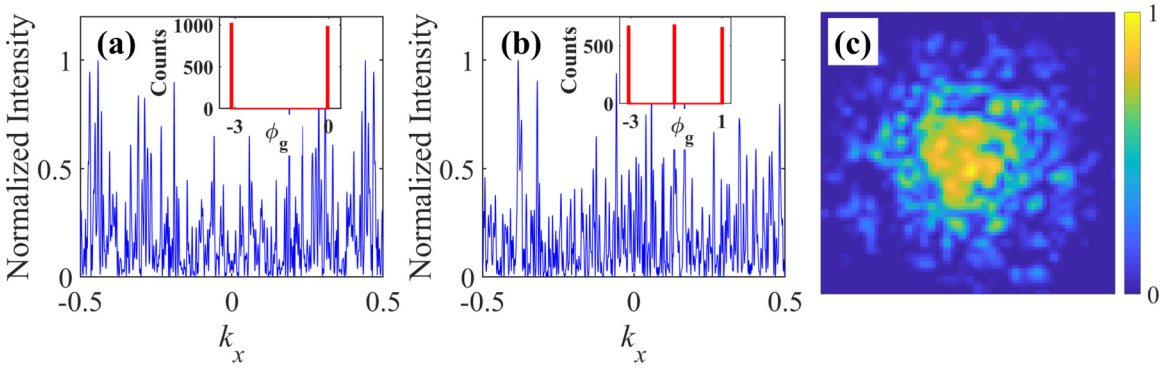

FIG. 7. The momentum distribution of the RCP polarization state (along k_x) obtained for a Gaussian beam transmitted from a disordered medium, where the individual anisotropic element gives a phase of (a) either 0 or $-\pi$ and (b) $-\pi$, $-\pi/3$, or $\pi/3$. (c) The momentum-space intensity distribution for the RCP polarization projection shows the random scattering modes for a binary distribution of gray level in 8×8 bins of the SLM.

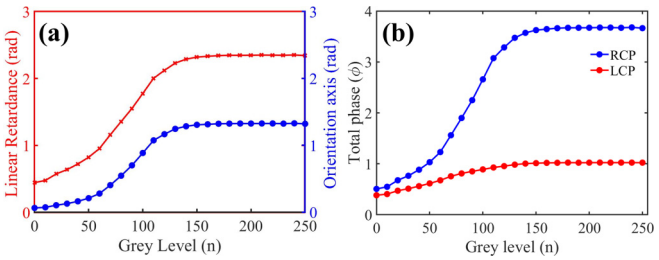

FIG. 8. The dependence of (a) polarization parameters and (b) the total phase ($\phi_d \pm \phi_g$) occupied by the light transmitted for input LCP and RCP polarization states of light on the gray level projected onto the SLM (adapted from Ref. [6]).

It can also be used to get a physical understanding of the critical range of the randomized phase value needed to observe the random optical Rashba effect.

APPENDIX B: MINIMUM NUMBER OF INDEPENDENT ELEMENTS REQUIRED FOR OBSERVING RANDOM SCATTERING MODES

Here, we show that completely random scattering modes in Fourier space by constructing the disordered system by randomly distributing the two optimum anisotropic units instead of various units with different geometric phases. Figure 7 shows the momentum space intensity distribution of the beam transmitted from a spatially disordered anisotropic medium consisting of only two orientations [$-\pi/2$ and 0, as shown in the inset Fig. 7(a)] of the half-wave-plate retarder (or geometric phases of $-\pi$ and 0) distributed randomly throughout space. In addition, we also show the momentum intensity distribution obtained by using only three optimum unit cells with different orientations of half-wave-plate retarders. The random scattering modes were also experimentally observed in scattering from the SLM for a given random binary distribution of gray levels for 8×8 bins of the SLM pixels, as shown in Fig. 7(c). The findings could be beneficial for making such random material by using experimental techniques such as focused ion beam lithography, electron-beam lithography, or any other material fabrication method.

APPENDIX C: THE POLARIZATION PARAMETERS OF THE SPATIAL LIGHT MODULATOR

Figure 8 shows the phase retardance and the orientation of a retarder formed at a given value of the gray level in the SLM. The value of the effective retardance and the effective orientation angle of the equivalent retarder is determined by the SLM's gray value, which regulates the voltage applied across the pixels of SLM. It is seen that, for a gray value in the range of 20 to 140, the retardance and the orientation angle are approximately linear and have the same slope with the SLM's gray level. The total phase occupied for the incident LCP and RCP polarization states of light with varying gray levels is shown in Fig. 8(b). The total phase occupied for the input RCP polarization state of light shows a significant dependence on the gray level of the SLM pixel compared with the LCP polarization state of light for which not much deviation is found with varying gray levels.

[1] K. Y. Bliokh, F. J. Rodríguez-Fortuño, F. Nori, and A. V. Zayats, Nat. Photonics **9**, 796 (2015).
[2] N. Shitrit, I. Yulevich, E. Maguid, D. Ozeri, D. Veksler, V. Kleiner, and E. Hasman, Science **340**, 724 (2013).
[3] S. Xiao, J. Wang, F. Liu, S. Zhang, X. Yin, and J. Li, Nanophotonics **6**, 215 (2017).
[4] X. Ling, X. Zhou, W. Shu, H. Luo, and S. Wen, Sci. Rep. **4**, 5557 (2014).
[5] X. Ling, X. Zhou, X. Yi, W. Shu, Y. Liu, S. Chen, H. Luo, S. Wen, and D. Fan, Light: Sci. Appl. **4**, e290 (2015).
[6] M. Pal, C. Banerjee, S. Chandel, A. Bag, S. K. Majumder, and N. Ghosh, Sci. Rep. **6**, 39582 (2016).
[7] X. Ling, X. Zhou, K. Huang, Y. Liu, C.-W. Qiu, H. Luo, and S. Wen, Rep. Prog. Phys. **80**, 066401 (2017).
[8] O. Hosten and P. Kwiat, Science **319**, 787 (2008).
[9] K. Y. Bliokh, D. Y. Frolov, and Y. A. Kravtsov, Phys. Rev. A **75**, 053821 (2007).
[10] L. Ma, S. Li, V. M. Fomin, M. Hentschel, J. B. Götte, Y. Yin, M. Jorgensen, and O. G. Schmidt, Nat. Commun. **7**, 10983 (2016).
[11] N. Shitrit, S. Maayani, D. Veksler, V. Kleiner, and E. Hasman, Opt. Lett. **38**, 4358 (2013).
[12] K. Frischwasser, I. Yulevich, V. Kleiner, and E. Hasman, Opt. Express **19**, 23475 (2011).
[13] E. Maguid, M. Yannai, A. Faerman, I. Yulevich, V. Kleiner, and E. Hasman, Science **358**, 1411 (2017).
[14] F. Wilczek and A. Zee, Phys. Rev. Lett. **52**, 2111 (1984).
[15] J. Zak, Europhys. Lett. **9**, 615 (1989).
[16] G. Garcia de Polavieja, Phys. Rev. Lett. **81**, 1 (1998).
[17] C. Loussert, U. Delabre, and E. Brasselet, Phys. Rev. Lett. **111**, 037802 (2013).
[18] L. Allen, S. M. Barnett, and M. J. Padgett, *Optical Angular Momentum* (CRC Press, Boca Raton, FL, 2003).
[19] S. D. Gupta, N. Ghosh, and A. Banerjee, *Wave Optics: Basic Concepts and Contemporary Trends* (CRC Press, Boca Raton, FL, 2015) .
[20] K. Dev and A. Asundi, Opt. Lasers Eng. **50**, 599 (2012).
[21] V. Duran, J. Lancis, E. Tajahuerce, and Z. Jaroszewicz, J. Appl. Phys. **97**, 043101 (2005).
[22] K. Lu and B. E. Saleh, Opt. Eng. **29**, 240 (1990).
[23] N. Bender, H. Yılmaz, Y. Bromberg, and H. Cao, Optica **5**, 595 (2018).
[24] G. Volpe, L. Kurz, A. Callegari, G. Volpe, and S. Gigan, Opt. Express **22**, 18159 (2014).
[25] J. Gateau, T. Chaigne, O. Katz, S. Gigan, and E. Bossy, Opt. Lett. **38**, 5188 (2013).
[26] F. Jendrzejewski, A. Bernard, K. Mueller, P. Cheinet, V. Josse, M. Piraud, L. Pezzé, L. Sanchez-Palencia, A. Aspect, and P. Bouyer, Nat. Phys. **8**, 398 (2012).
[27] T. Chaigne, J. Gateau, M. Allain, O. Katz, S. Gigan, A. Sentenac, and E. Bossy, Optica **3**, 54 (2016).